ARCHITECTURE CIVIL ENGINEERING ENVIRONMENT
The Silesian University of Technology No. 2/2012

THE EFFECT OF AGGREGATE CHARACTERISTICS ON THE FRACTURE BEHAVIOUR OF FINE-GRAINED CONCRETE UNDER TENSILE LOADING

Łukasz SKARŻYŃSKI [a], Jacek TEJCHMAN [b]

[a] Dr.; Faculty of Civil and Environmental Engineering, Gdańsk University of Technology, Poland
E-mail address: *lskarzyn@pg.gda.pl*

[b] Prof.; Faculty of Civil and Environmental Engineering, Gdańsk University of Technology, Poland
E-mail address: *tejchmk@pg.gda.pl*

Received: 10.03.2012; Revised: 30.04.2012; Accepted: 15.06.2012

Abstract
This paper presents the effect of the aggregate characteristics on the fracture behaviour of fine-grained concrete under quasi-static three-point bending. Concrete was modelled as a random heterogeneous three-phase material. The 2D simulations for notched concrete beams were carried out with the finite element method using an isotropic damage constitutive model enhanced by a characteristic length of micro-structure by means of a non-local theory. The effect of the volume fraction, shape, size and statistical distribution of aggregate was analysed. The numerical results were compared with own laboratory test results and other meso-scale calculations for three-phase concrete elements.

Streszczenie
Artykuł przedstawia analizę wpływu kruszywa na zjawisko pękania drobnoziarnistego betonu podczas quasi-statycznego trzypunktowego zginania. Beton został opisany jako stochastyczny i niejednorodny materiał trzyfazowy. Dwuwymiarowe obliczenia numeryczne dla betonowych belek z nacięciem wykonano metodą elementów skończonych stosując izotropowy materiałowy model z degradacją sztywności rozszerzony o długość charakterystyczną mikrostruktury przy zastosowaniu teorii nielokalnej. Analizowano wpływ procentowej zawartości, kształtu, wielkości i rozkładu losowego ziaren kruszywa. Wyniki obliczeń numerycznych porównano z wynikami własnych badań laboratoryjnych oraz podobnych obliczeń numerycznych dla trzyfazowych elementów betonowych.

Keywords: **Aggregate; Concrete; Damage Model; Finite Element Analysis; Mesoscopic; Approach; Microstructure.**

1. INTRODUCTION

An understanding of the mechanism of the formation of localized zones (width and spacing) in concrete materials is crucial to evaluate the mobilized material strength close to the peak and in the post-peak regime and the related size effect, and thus to ensure safety to the civil engineering structures (Bažant and Planas [1]). The mechanism of strain localization strongly depends upon a heterogeneous structure of materials over many different scales, changing e.g. in concrete from the few nanometers (hydrated cement) to the millimetres (aggregate particles). Therefore, to take strain localization into account, material composition (micro-structure) has to be taken into account (Bažant and Planas [1], Lilliu and van Mier [2], Nielsen et al. [3], Sengul et al. [4], Kozicki and Tejchman [5], He [6]). At the meso-scale, concrete can be considered as a composite material by distinguishing 3 important phases: cement matrix, aggregate and interfacial transition zones ITZs. In particular, the presence of aggregate and ITZs is important since the volume fraction of aggregate can be as high as 70-75% in concrete and ITZs are always the weakest regions in concrete. The concrete behaviour at the meso-scale fully determines the macroscopic non-linear behaviour. The advantage of meso-scale modelling is the fact that it directly simulates micro-structure and can be used to comprehensively study local phenomena at the micro-level such as the mechanism of the initiation, growth and formation of localized zones and cracks (He [6], Kim and Abu Al-Rub [7], Shahbeyk et al. [8]). Through that the mesoscopic results allow for a better calibration of continuum models enhanced by micro-structure and an optimization design of concrete with enhanced strength and ductility. The disadvantages are: very high computational cost, inability to model aggregate shape accurately and the difficulty to experimentally measure the properties of ITZs. The concrete behaviour at the meso-scale can be described with continuum and discrete models. In this study we used an enhanced continuum approach.

The intention of our 2D meso-mechanical continuum calculations is to investigate the effect of the aggregate characteristics on the fracture behaviour of a fine-grained notched concrete beam under tensile loading during quasi-static three-point bending. Concrete was modelled as a random heterogeneous three-phase material. To obtain mesh-objective FE results for concrete specimens with localized zones, a simple isotropic continuum constitutive damage model (Marzec et al. [9], Skarżyński and Tejchman [10]) enhanced by a characteristic length of micro-structure by means of a non-local theory (Pijauder-Cabot and Bažant [11], Bažant and Jirasek [12], Bobiński et al. [13]) was used. The effect of meso-structural features such as volume fraction, shape, size, statistical distribution and grading curve of aggregate was carefully analysed. The results of our mesoscopic level analyses were directly compared with corresponding laboratory test results with notched concrete beams, where the width, length and shape of a localized zone on the surface of notched concrete beams was determined with a Digital Image Correlation (DIC) technique (Skarżyński et al. [14]).

2. CONSTITUTIVE MODEL FOR CONCRETE

A simple isotropic damage continuum model was used for describing the material degradation with the aid of a single scalar damage parameter D, growing monotonically from zero (undamaged material) to one (completely damaged material) (Katchanov [18], Simo and Ju [19]). The relationship between the stress σ_{ij} and strain tensor ε_{kl} is

$$\sigma_{ij} = (1-D)C^e_{ijkl}\varepsilon_{kl}\,, \tag{1}$$

where D denotes the scalar damage parameter growing monotonically from zero (undamaged material) to one (completely damaged material) and C^e_{ijkl} is the linear elastic material stiffness matrix. The loading function of damage is as follows

$$f(\tilde{\varepsilon},\kappa) = \tilde{\varepsilon} - \max\left\{\kappa,\kappa_0\right\}, \tag{2}$$

where κ_0 denotes the initial value of κ when damage begins. If the loading function f is negative, damage does not develop. During monotonic loading, the parameter κ grows (it coincides with $\tilde{\varepsilon}$) and during unloading and reloading it remains constant. A Rankine failure type criterion was assumed to define the equivalent strain measure $\tilde{\varepsilon}$ (Jirasek and Marfia [20])

$$\tilde{\varepsilon} = \frac{\max\left\{\sigma_i^{eff}\right\}}{E}, \tag{3}$$

where E denotes the modulus of elasticity and σ_i^{eff} are the principal values of the effective stress tensor

$$\sigma_{ij}^{eff} = C^e_{ijkl}\varepsilon_{kl}\,. \tag{4}$$

If all principal stresses are negative, the loading function f is negative and no damage takes place.

To describe the evolution of the damage parameter D determining the shape of a softening curve during tensile loading, the exponential law was used (Peerlings et al. [21])

$$D = 1 - \frac{\kappa_0}{\kappa}\left(1-\alpha+\alpha e^{-\beta(\kappa-\kappa_0)}\right), \tag{5}$$

where α and β are the material constants. The constitutive isotropic damage model for concrete requires 5 material constants only (2 elastic and 3 plastic): E, ν, κ_0, α and β. The model is mainly suitable for tensile failure in quasi-brittle materials (Marzec et al. [9], Skarżyński et al. [14]). Its disadvantages are that it cannot realistically describe irreversible deformations, volume changes and shear failure.

To capture strain localization in concrete, to obtain mesh-independent results and finally to include a characteristic length of micro-structure l_c (which determines the width of a localized zone), an integral-type non-local theory was used in FE simulations as a regularization technique (Bažant and Jirasek [12], Bobiński and Tejchman [25]). The equivalent strain measure $\tilde{\varepsilon}$ was replaced by its non-local value

$\tilde{\varepsilon}$ (Pijauder-Cabot and Bažant [11]) to evaluate the loading function (Eq.2) and to calculate the damage threshold parameter κ

$$\bar{\varepsilon} = \frac{\int_V \omega(\|x-\xi\|)\tilde{\varepsilon}(\xi)\,d\xi}{\int_V \omega(\|x-\xi\|)\,d\xi}, \tag{6}$$

where V – the body volume, x – the coordinates of the considered (actual) point, ξ – the coordinates of surrounding points and ω – the weighting function. As a weighting function ω, the Gauss distribution function was used

$$\omega(r) = \frac{1}{l_c\sqrt{\pi}} e^{-\left(\frac{r}{l_c}\right)^2}, \tag{7}$$

where the parameter r is a distance between two material points. The averaging in Eq. 7 is restricted to a small representative area around each material point (the influence of points at the distance of $r=3\times l_c$ is only 0.01%). To obtain fully mesh-objective FE results, the maximum size of finite elements should be equal to (2-3)$\times l_c$ (Bobinski and Tejchman [25]). A characteristic length is usually related to material micro-structure and is determined with an inverse identification process of experimental data (Le Bellĕgo et al. [26], Skarzyński et al. [14]). The FE calculations were carried out using a large-displacement analysis. The non-local averaging was performed in the current configuration.

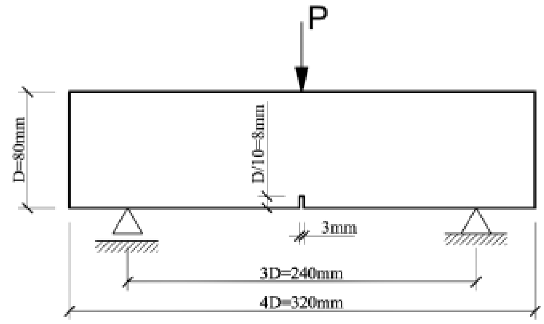

Figure 1.
Geometry of small-size notched concrete beam with thickness of 40 mm subjected to quasi-static three-point bending used in tests by Le Bellĕgo et al. [26] and Skarżyński et al. [14] (P – vertical force, D =80 mm – beam height)

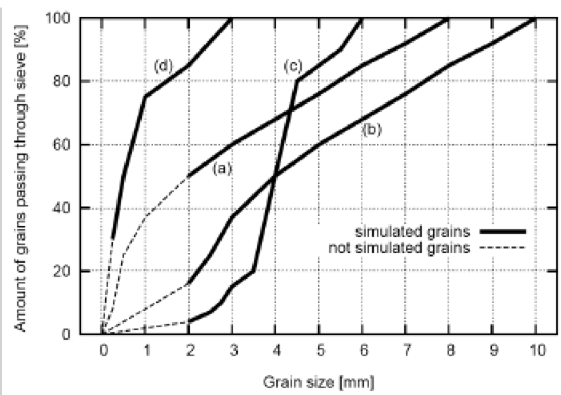

Figure 2.
Aggregate size distribution curves assumed for FE calculations (note that small aggregates were cut off to reduce the computation time)

3. INPUT DATA FOR MESOSCOPIC FE CALCULATIONS

Two-dimensional mesoscopic FE simulations were performed with a small-size notched free-supported beam made from fine-grained concrete (80×320×40 mm^3) subjected to quasi-static three-point bending (Fig. 1). The same concrete beam was experimentally investigated by Le Bellĕgo et al. [26]) and by Skarżynski et al. [14] in size effect tests. The beam was subjected to a vertical displacement at the top mid-point at a very slow rate. Concrete at the meso-scale was considered as a three-phase material encompassing cement matrix, aggregate and interfacial transition zones (ITZs) between cement matrix and aggregate. Four different fine-grained concrete mixes were numerically analysed with the mean aggregate size d_{50}=2 mm, d_{50}=4 mm, d_{50}=4 mm and d_{50}=0.5 mm, respectively (Fig. 2). To reduce the number of aggregate grains in calculations, the size of the smallest inclusions had to be limited (Fig. 2). The final aggregate size varied between the minimum value d_{min}=2 mm and maximum value d_{max}=8 mm (aggregate size distribution curve "a" of Fig. 2), d_{min}=2 mm and d_{max}=10 mm (aggregate size distribution curve "b" of Fig. 2), d_{min}=2 mm and d_{max}=6 mm (aggregate size distribution curve "c" of Fig. 2) and d_{min}=0.25 mm and d_{max}=3 mm (aggregate size distribution curve "d" of Fig. 2). The aggregate was generated according to the method given by Eckardt and Könke [27]. The aggregate was randomly placed starting with the largest ones and preserving a certain mutual distance (van Mier et al. [28])

$$D_p > 1.1\frac{D_1 + D_2}{2}, \tag{8}$$

where D_p is the distance between two neighbouring particle centres and D_1, D_2 are the diameters of two

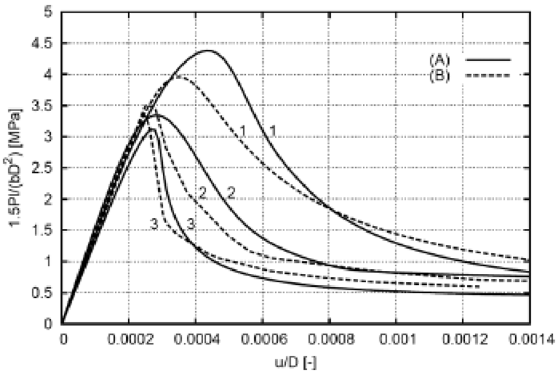

Figure 3.
Calculated nominal strength 1.5*Pl*/(*bD*^{2}) versus normalised beam deflection *u*/*D* (*P* – vertical force, *u* – beam deflection, *D* – beam height, *b* – beam width, *l* – beam span): A) mesoscopic FE results, B) experiments by Le Bellĕgo et al. [26]: 1) small-size beam 80×320 40 mm^3, 2) medium-size beam 160×640×40 mm^3, 3) large-size beam 320×1280×40 mm^3 (three-phase random heterogeneous fine-grained concrete with characteristic length of micro-structure of 1.5 mm) (Skarżyński and Tejchman [14])

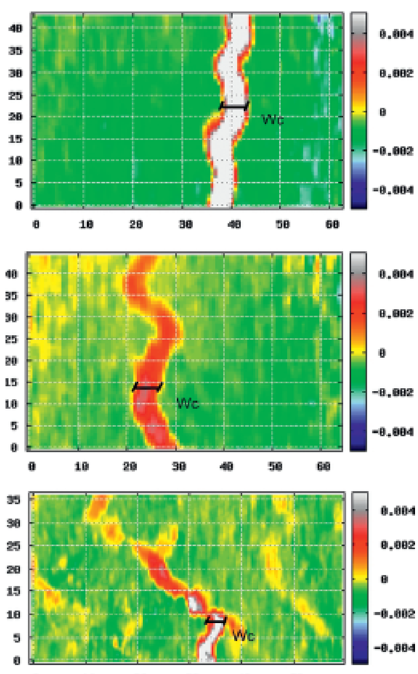

Figure 4.
Formation of localized zone with mean width of w_c=3.5-4.0 mm directly above notch in 3 different experiments with small-size notched beam 80×320×40 mm^3 using DIC (vertical and horizontal axes denote coordinates in [mm] and colour scales strain intensity) (Skarżyński et al. [14])

particles, respectively. The aggregate volume fraction was ρ = 30%, ρ = 45% or ρ = 60%.

For the sake of simplicity, the FE calculations were carried out with one set of the material constants E, ν, κ_0, α, β and l_c given in Tab.1, which were prescribed to finite elements corresponding to a specified concrete phase. These material constants were determined with the aid of comparative FE analyses of both the load-deflection curves and width of a localized zone above the notch with corresponding laboratory experiments (Le Bellĕgo et al. [26] and Skarżynski et al. [14]) which were carried out with 3 geometrically similar notched beams using fine-grained concrete (with d_{max}=8.0 mm and d_{50}=2.0 mm corresponding to the curve “a” of Fig. 2) and very fine-grained concrete (with d_{max}=3.0 mm and d_{50}=0.5 mm corresponding to the curve “d” of Fig. 2) (Figs. 3 and 4) (Skarżyński and Tejchman [10]). The modulus of elasticity E and crack initiation strain κ_0 were solely changed in 3 phases (the remaining constants were the same: υ=0.2, α=0.95, β=200 and the mesoscopic characteristic length l_c^m=1.5 mm). In turn, the macroscopic calculations for a homogeneous concrete material were carried out with the following material constants: E=38.5 GPa, ν=0.2, κ_0=1.3×10^{-4}, α=0.95, β=400 and the macroscopic characteristic length l_c=2 mm (Skarżyński and Tejchman [10]). In general, the material constants should be determined with laboratory tensile tests for each phase (that is certainly possible for aggregate and cement matrix but not feasible for ITZs). Since the material constants for aggregate and cement matrix were not separately determined with laboratory experiments, other relationships between material constants E and κ_0 were also possible to obtain a satisfactory agreement between experiments and FE analyses. ITZ was assumed to be the weakest component where damage was always initiated (Lilliu and van Mier [2], Kozicki and Tejchman [5]). The FE-meshes included up to 560’000 triangular elements. The size of finite elements was small enough to obtain mesh-objective numerical results: s_a=0.5 mm (aggregate), s_{cm}=0.1-0.2 mm (cement matrix) and s_{ITZ}=0.1 mm (ITZ). Due to the fact that the measured width of a localized zone was slightly dependent upon the concrete mix (Skarżyński et al. [14]), the mesoscopic characteristic length l_c^m was simply imposed so that the numerical results agreed with the experimental observations. In our future numerical investigations, it will be related to concrete microstructure (aggregate size or aggregate spacing).

Typical experimental force-deflection curves with notched beams of fine-grained concrete obtained in experiments by Le Bellĕgo et al. [26] and in FE mesoscopic analyses by Skarżyński and Tejchman [10] are presented in Fig. 3 (the maximum vertical force occurred at the beam deflection of u=0.02-0.03 mm). In turn, Fig. 4 shows the formation of a localized zone on one side of the surface of a fine-grained small-size concrete beam above the notch from laboratory tests by Skarżyński et al. [14] using a Digital Image Correlation technique DIC, which is an optical way to visualize surface displacements by successive post-processing of digital images taken at a constant time increment from a professional digital camera (based on displacements, strains can be calculated). A localized zone occurred always before the peak on the force-deflection diagram and was strongly curved. In some cases, it branched. The measured width of a localized zone above the notch increased during deformation due to concrete dilatancy (Fig. 5A) up to w_c=3.5-4.0 mm ($\le d_{max}$) in the range of the deflection u=0.01-0.04 mm until a macro-crack was created. The maximum height of a localized zone above the notch was about h_c=50-55 mm at u=0.04 mm (Fig. 5B). The width of a localized zone slightly depended upon the concrete mix type and beam size (Skarżyński et al. [14]).

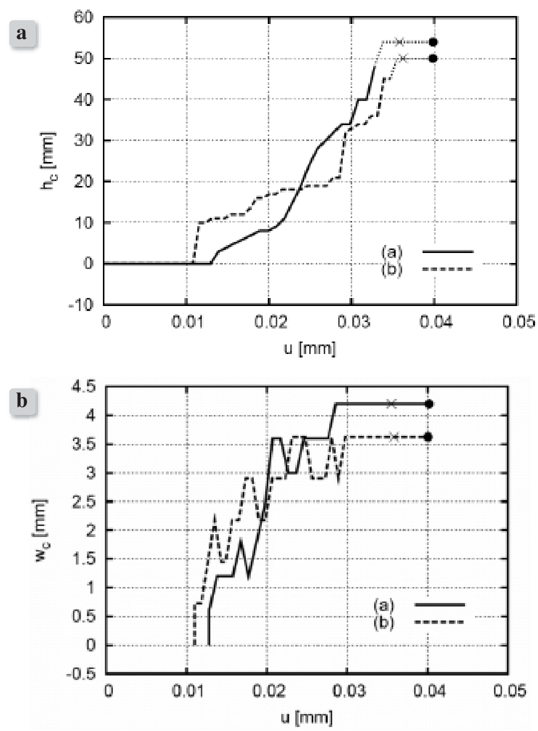

Figure 5.
Evolution of width w_c (A) and height h_c (B) of localized zone with deflection u directly above notch in experiments with small-size notched beam 80×320×40 mm^3 of fine-grained concrete using DIC: a) aggregate d_{50}=2 mm and d_{max}=8 mm, b) aggregate d_{50}=0.5 mm and d_{max}=3 mm (× - maximum vertical force, • - formation of macro-crack)

The beam was modelled as a partially homogeneous and partially heterogeneous with a meso-section in the neighbourhood of the notch to reduce the computation time (Fig. 6). Based on earlier FE calculations, the minimum width of the heterogeneous region $b_{ms}=D$ near the notch should be equal to beam height D in order to obtain similar results as in the entirely heterogeneous beam (Skarżyński and Tejchman [10]).

The calculated width of a localized zone above the notch was determined at the beam deflection of u=0.15 mm based on the non-local softening strain measure $\bar{\varepsilon}$ (Eq.6). As the cut-off value $\bar{\varepsilon}_{min}$ =0.025 was always assumed at the maximum mid-point value of $\bar{\varepsilon}_{max}$=0.08-0.13.

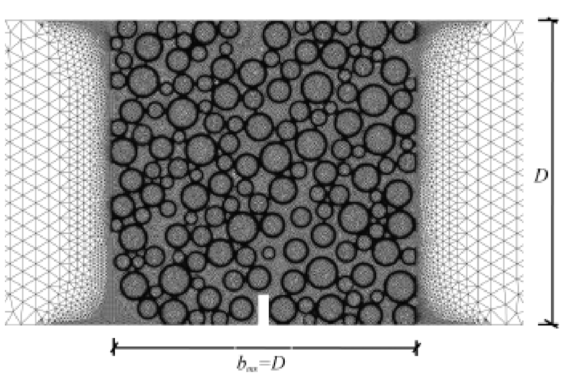

Figure 6.
FE mesh: three-phase heterogeneous concrete in notch neighbourhood with round shaped aggregate, cement matrix and interfacial transition zones ITZ and one-phase homogeneous concrete in remaining region

4. MESOSCOPIC FE RESULTS

Below the numerical 2D effect of different parameters such as the aggregate distribution, aggregate volume and aggregate shape on the material behaviour (load-deflection curve and strain localization) is described. The parameters were varied independently.

4.1. Effect of stochastic aggregate distribution

The effect of a random distribution of round-shaped aggregate particles in the concrete beam on the force-deflection diagram and width of a localized zone is shown in Figs. 7 and 8. The aggregate volume was ρ=45% using two aggregate size distribution curves "a" (d_{min}=2 mm, d_{max}=8 mm) and "d" (d_{min}=0.25 mm, d_{max}=3 mm) of Fig. 2, respectively. The ITZ thickness was always t_b=0.25 mm (Gitman et al. [15]).

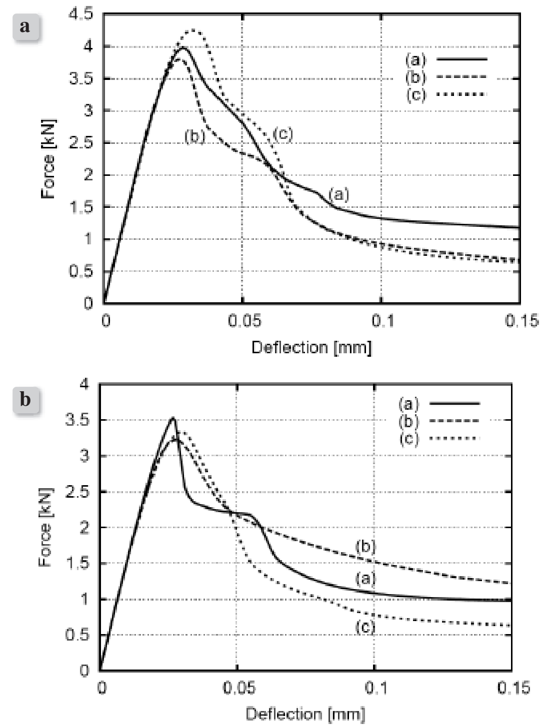

Figure 7.
Calculated force-deflection curves for fine-grained concrete beam (l_c^m=1.5 mm, ρ=45%, t_b=0.25 mm): A) with aggregate size distribution curve "a" of Fig. 2 (d_{min}=2 mm and d_{max}=8 mm) and B) with aggregate size distribution curve "d" of Fig. 2 (d_{min}=0.5 mm and d_{max}=3 mm) for three random distributions of circular aggregates (curves "a", "b" and "c")

All stochastic force-deflection curves are obviously the same in the almost entire elastic regime. However, they are significantly different at and after the peak (Fig. 7) due to a localized zone propagating between aggregate distributed at random, which is always non-symmetric and curved (Fig. 8). The difference in the strength is about 10-20%. The calculated width of a localized zone is approximately w_c=4.5 mm=3×l_c^m=9×s_{cm} independently of d_{min} and d_{max} (as in our tests, Skarżyński et al. [14]). The calculated localized zone is created at about u/D=0.0003 (u=0.024 mm) and its width increases during the deformation process.

A similar strong stochastic effect was also observed in FE calculations by Gitman et al. [15] and He [6]. Surprisingly, a negligible stochastic effect was found in FE simulations by Kim and Abu Al-Rub [7].

4.2. Effect of aggregate shape and aggregate size distribution

To model the effect of the aggregate shape, four different grain shapes were taken into account, namely: circular, octagonal, irregular (angular) and rhomboidal (Fig. 9) keeping always the volume fraction and centres of grains constant (l_c^m=1.5 mm, ρ=60%, t_b=0.25 mm).

The aggregate shape can have a different influence on the beam ultimate strength depending upon the aggregate size distribution (Figs. 10 and 11). For the aggregate size distribution of Fig. 2a, the ultimate beam strength is the highest for rhomboidal-shaped particles and the lowest for octagonal-shaped parti-

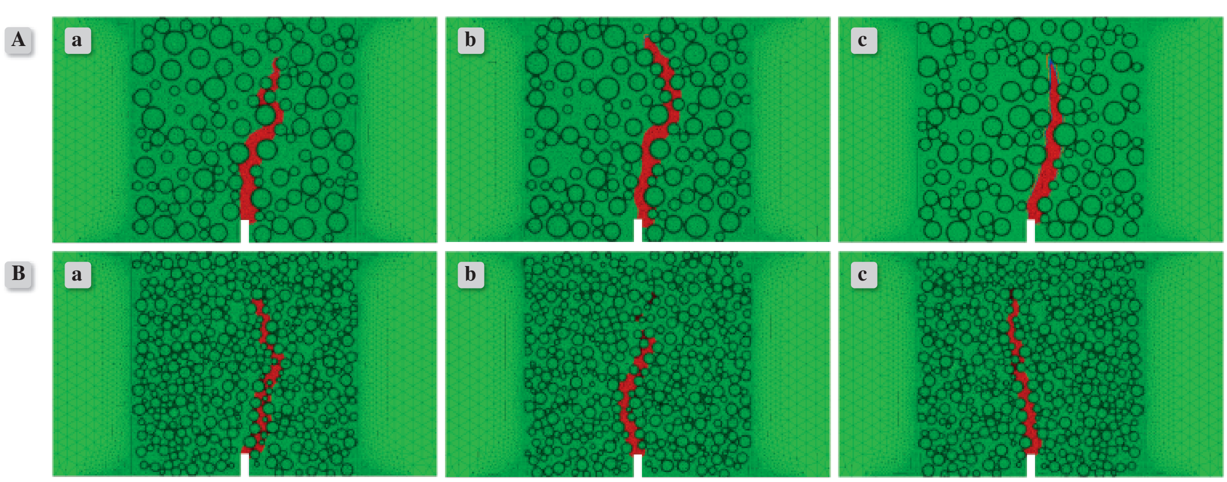

Figure 8.
Calculated localized zone in fine-grained concrete beam in notch region based on distribution of non-local strain measure corresponding to load-deflection curves 'a', 'b' and 'c' of Figs.7A and 7B (l_c^m=1.5 mm, ρ=45%, t_b=0.25 mm)

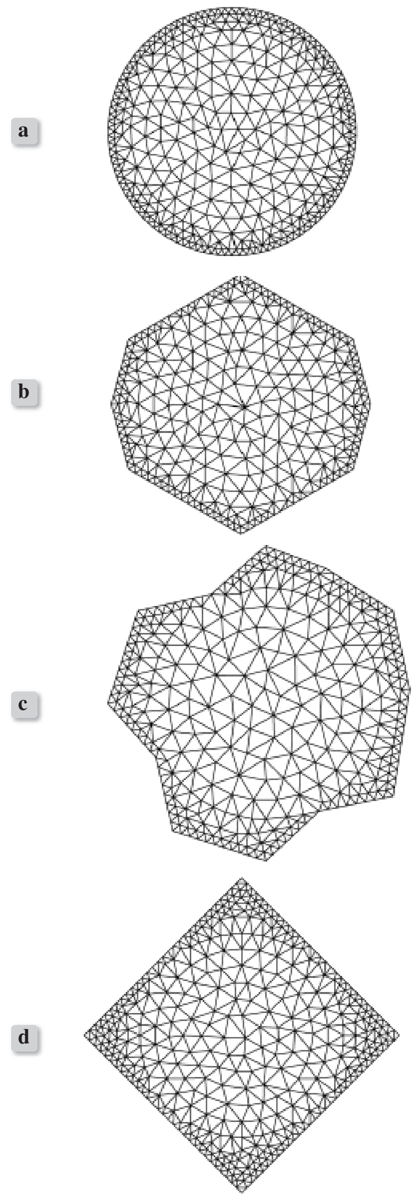

Figure 9.
Aggregate shape assumed in calculations: a) circular, b) octagonal, c) irregular (angular), d) rhomboidal

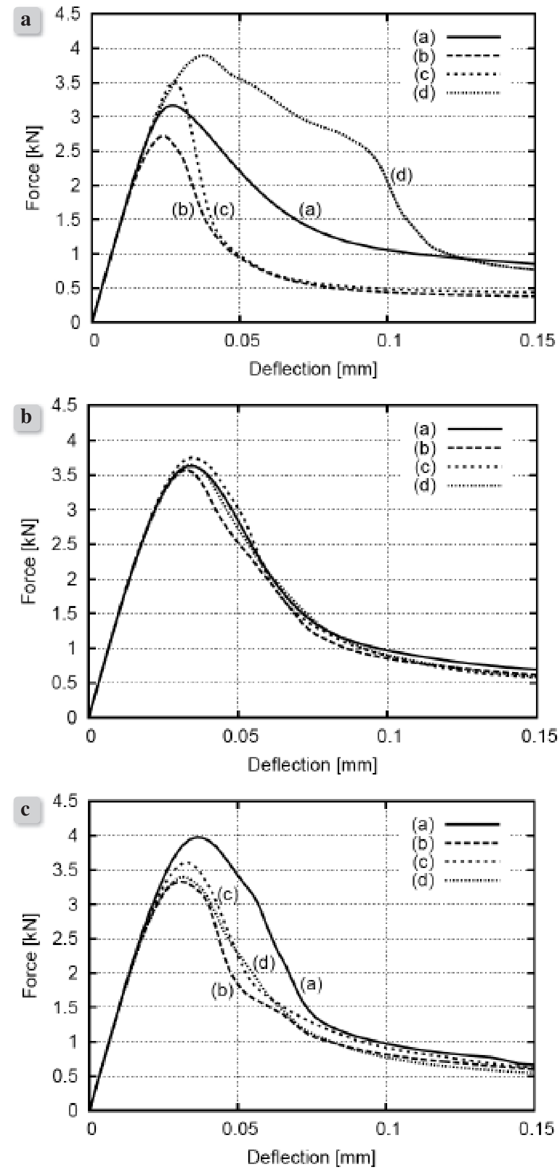

Figure 10.
Calculated force-deflection curves for different aggregate shape of Fig.9: a) circular, b) octagonal, c) irregular (angular), d) rhomboidal (fine-grained concrete beam 80 320 mm^2, l_c^m=1.5 mm, ρ=60%, t_b=0.25 mm) and different aggregate size distributions of Fig.2: A) d_{min}=2 mm and d_{max}=8 mm (curve "a"), B) d_{min}=2 mm and d_{max}=10 mm (curve "b"), C) d_{min}=2 mm and d_{max}=6 mm (curve "c")

cles (Fig. 9a, Figs. 11b and 11d). This difference equals even 30%. In case of the aggregate size distribution curve of Fig. 2b, the ultimate beam strength is similar for all assumed particle shapes (Fig. 10b). For the aggregate size distribution of Fig. 2c, angular-shaped inclusions have the lower tensile strength than circular grains (Fig. 10c). From simulations follows that the mean tensile strength is usually higher with the larger mean grain size and the narrower grain range (Figs. 10a, 10b, 10c and 11).

The width of a localized zone equals approximately w_c=3 mm for ρ=60% and is not influenced by the aggregate shape, aggregate distribution, mean and maximum grain size (Fig. 12). In turn, the form of a localized zone is strongly affected by the aggregate shape contributing thus to the different strength. The calculated width of a localized zone is in good agree-

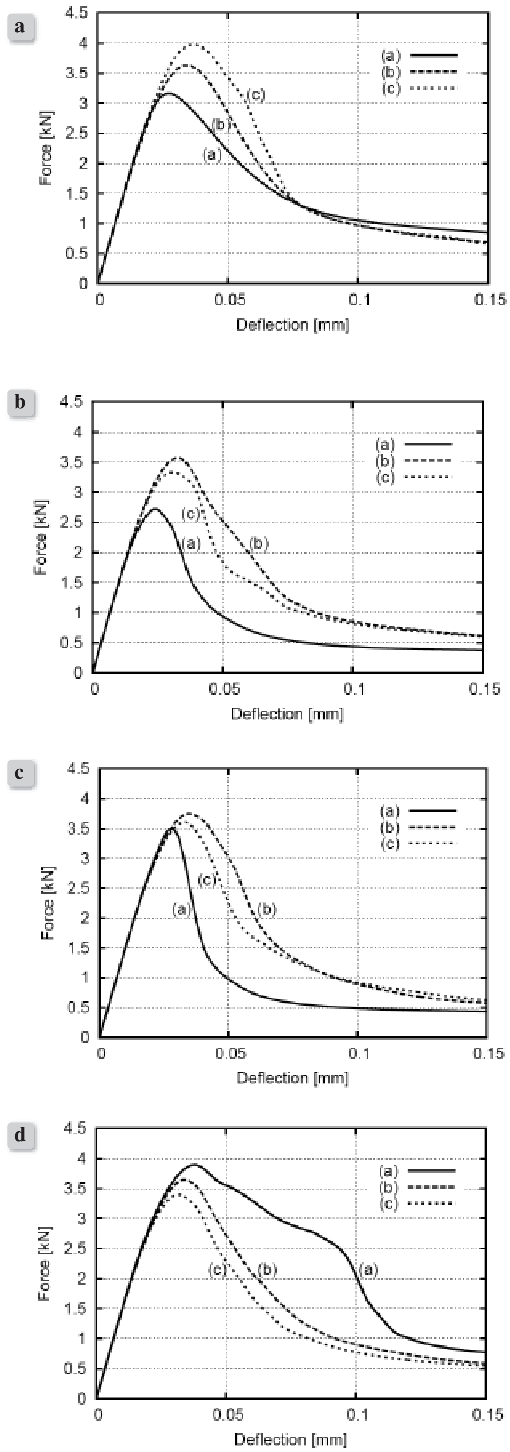

Figure 11.
Calculated force-deflection curves for different aggregate shape of Fig. 9: a) circular, b) octagonal, c) irregular (angular), d) rhomboidal (fine-grained concrete beam 80×320 mm^2, l_c^m=1.5 mm, ρ=60%, t_b=0.25 mm) and different aggregate size distribution of Fig.2: a) d_{min}=2 mm and d_{max}=8 mm (curve "a"), b) d_{min}=2 mm and d_{max}=10 mm (curve "b"), c) d_{min}=4 mm and d_{max}=6 mm (curve "c")

ment with our experiments with fine-grained concrete (Figs. 4 and 5A). Our outcome is in contrast to statements by Pijauder-Cabot and Bažant [11], and Bažant and Oh [30] wherein the width of a localized zone in usual concrete was estimated to be dependent upon d_{max}. It is also in contrast to experimental results by Mihashi and Nomura [31] which showed that the width of a localized zone in usual concrete increased with increasing aggregate size. The differences between our and the experimental results (Bažant and Oh [30], Mihashi and Nomura [31]) lie probably in a different concrete mix, specimen size and loading type. For instance, in our other tests with large reinforced concrete beams 6.0 m long without shear reinforcement under bending, the width of a localized zone in usual concrete was about 15 mm indicating that l_c=5 mm (Syroka and Tejchman [32]). This problem merits further experimental and numerical investigations.

According to Kim and Abu Al-Rub [7] the aggregate shape has a weak effect on the ultimate strength of concrete and on the strain to damage-onset, but significantly affects the crack initiation, propagation and distribution. The stress concentrations at sharp edges of polygonal particles cause that the ultimate tensile strength and strain at the damage onset are the highest for circular grains model. Similar conclusions were derived by He et al. [17] and He [6].

3.3. Effect of volume fraction of aggregate

Circular grains with the volume of ρ=30%, ρ=45% and ρ=60% were used (l_c^m=1.5 mm and t_b=0.25 mm). Figures 13 and 14 demonstrate the effect of the aggregate volume in fine-grained concrete beam with the aggregate size distributions "a" of Fig.2 (d_{min}=2 mm, d_{max}=8 mm) and "d" of Fig. 2 (d_{min}=0.25 mm, d_{max}=3 mm).

In our FE simulations, the Young modulus and ultimate beam strength increase with increasing aggregate density in the range of 30%-60% (Fig. 13). This increase certainly depends on material parameters assumed for separated concrete phases, in particular for ITZs being always the weakest parts in concrete.

The width and shape of a localized zone are influenced by the aggregate volume; a localized zone becomes narrower with increasing aggregate volume: w_c=6 mm at ρ=30%, w_c=4.5 mm at ρ=45% and w_c=3 mm at ρ=60% (Fig. 14).

According to Kim and Abu Al-Rub [7] the Young modulus linearly increases with increasing aggregate

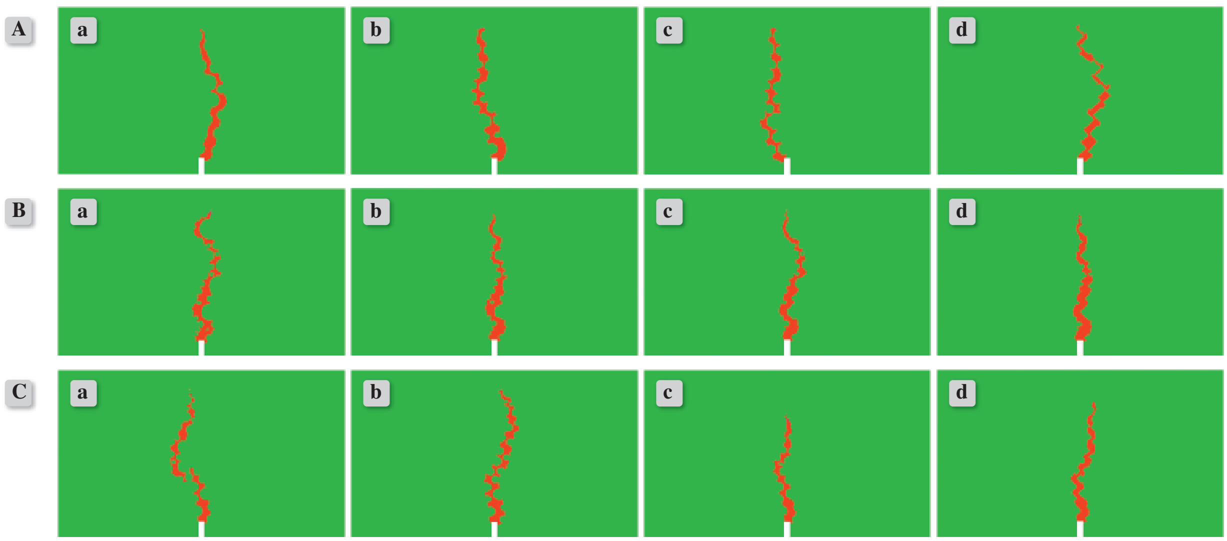

Figure 12.
Calculated localized zone based on distribution of non-local strain measure in fine-grained concrete beam in notch region corresponding to load-deflection curves "a", "b", "c" and "d" of Figs.10A, 10B and 10C (l_c^m=1.5 mm, ρ=60%, t_b=0.25 mm)

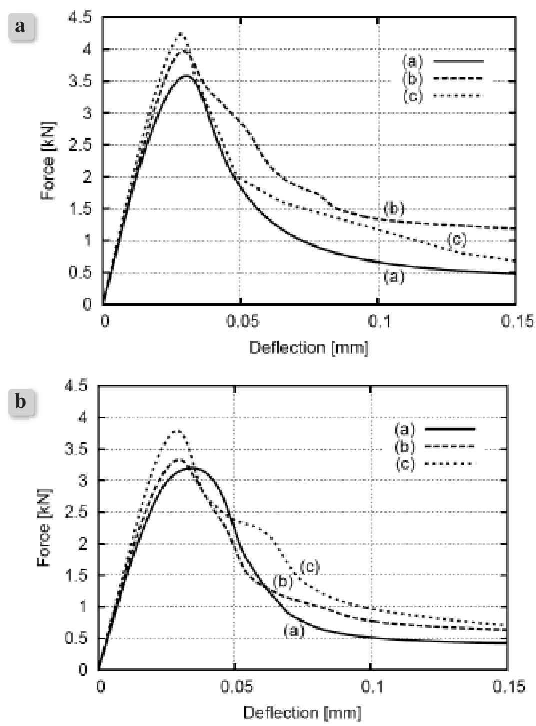

Figure 13.
Calculated load-deflection curves for different volume fractions of circular aggregate: a) ρ=30%, b) ρ=45% and c) ρ=60% (concrete beam 80×320 mm², l_c^m=1.5 mm, t_b=0.25 mm, A) aggregate size distribution "a" of Fig. 2 (d_{min}=2 mm, d_{max}=8 mm), B) aggregate size distribution "d" of Fig. 2 (d_{min}=0.5 mm, d_{max}=3 mm)

volume, and the tensile strength decreases with increasing aggregate density up to ρ=40% and increases next from ρ=40% up to ρ=60%. The strain at the damage linearly decreases with increasing aggregate volume. He et al. [17] and He [6] concluded that concrete with a higher packing density of aggregate up to 50% has a decreasing tensile strength (due to a higher number of very weak interfacial transitional zones around aggregate). It seems that the property of ITZ (stiffness, strength and width) is essential for the global strength versus ρ.

Finally, Fig. 15 shows the evolution of the width and height of the localized zone from FE calculations. The FE results of Fig. 23 are similar as in the experiments (Fig. 5). The calculated maximum width is 3.25 mm (3.5-4.0 mm in tests) and height 55 mm (50-55 mm in tests) at u=0.2 mm. The calculated localized zone linearly forms before and after the maximum vertical force in the range of u=0.025-0.05 mm (width) and of u=0.025-0.1 mm (length). The mean propagation rate of the calculated localized zone versus the beam deflection is similar as in experiments, although is more uniform (Fig. 16). In the experiments, a macro-crack occurred at about u=0.04 mm, which cannot be captured by our model. In order to numerically describe a macro-crack, a discontinuous approach has to be used (e.g. XFEM or cohesive crack model [35], [36], [37]).

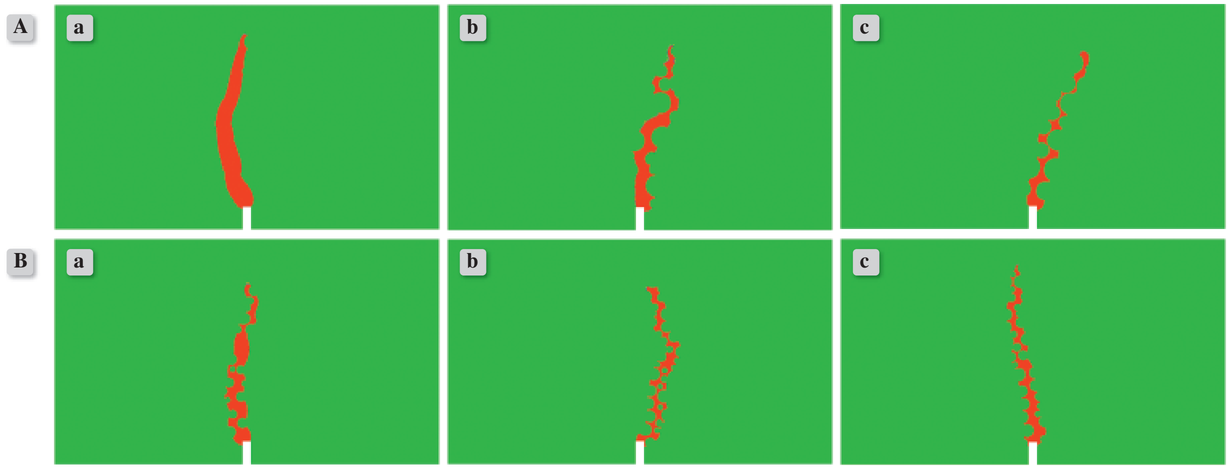

Figure 14.
Calculated localized zone based on distribution of non-local strain measure in fine-grained concrete beam 80×320 mm² (l_c^m=1.5 mm, t_b=0.25 mm) corresponding to load-deflection curves "a", "b" and "c" of Figs. 14A and 14B

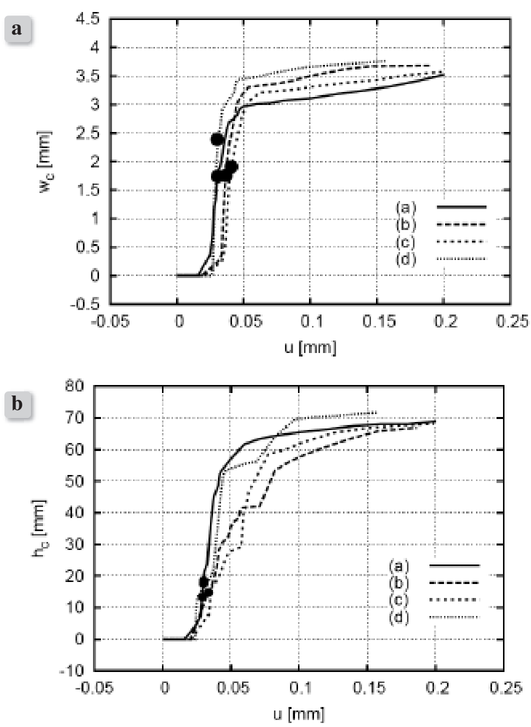

Figure 15.
The calculated evolution of width (A) w_c and height h_c (B) of localized zone versus beam deflection u: a) concrete mix "a" of Fig. 2 with d_{min}=2 mm and d_{max}=8 mm, irregular aggregate, =60%, l_c^m=1.5 mm, b) concrete mix "b" of Fig. 2 with d_{min}=2 mm and d_{max}=10 mm, octagonal aggregate, ρ=60%, l_c^m=1.5 mm, c) concrete mix "c" of Fig. 2 with d_{min}=2 mm and d_{max}=6 mm, circular aggregate, ρ=60%, l_c^m=1.5 mm, d) concrete mix "a" of Fig.2 with d_{min}=2 mm and d_{max}=8 mm, circular aggregate, ρ=60%, beam without notch, l_c^m=1.5 mm (• – maximum vertical force)

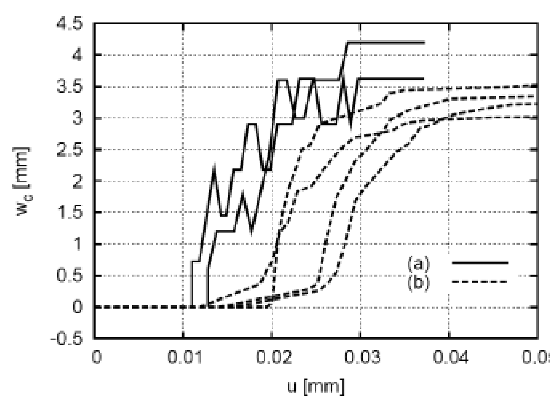

Figure 16.
Comparison between measured (a) and calculated (b) evolution of width of localized zone w_c versus beam deflection u (maximum vertical force occurs at deflection u=0.035 mm)

Table 1.
Material parameters assumed for FE calculations of concrete notched beams under bending at meso-scale (Skarżyński and Tejchman [10])

Parameters	Aggregate	Cement matrix	ITZ
Modulus of elasticity E [GPa]	40	35	30
Poisson's ratio ν [-]	0.2	0.2	0.2
Crack initiation strain κ_0 [-]	0.5	1 x 10^{-4}	7 x 10^{-4}
Residual stress level α [-]	0.95	0.95	0.95
Slope of softening β [-]	200	200	200
Mesoscopic characteristic length l_c^m [mm]	1.5	1.5	1.5

5. CONCLUSIONS

The following conclusions can be drawn from 2D calculations with notched fine-grained concrete beams under quasi-static three-point bending using a simplified meso-scale numerical model (by neglecting small aggregate grains):

- material micro-structure at meso-scale has to be taken into account in calculations of strain localization to obtain a proper shape of a propagating localized zone,
- the calculated strength, width and shape of a localized zone are in a satisfactory agreement with our size effect experiments when the characteristic length of micro-structure is 1.5 mm,
- the load-displacement evolutions strongly depend on material parameters assumed for separated concrete phases and a statistical distribution of aggregate. The ultimate beam strength certainly increases with increasing mean aggregate size. It may increase with increasing volume fraction of aggregate. It is also dependent upon the aggregate shape,
- the width of a localized zone increases with decreasing aggregate volume. It is not affected by the aggregate size, aggregate shape and stochastic aggregate distribution. The width of a calculated localized zone above the notch changes from about $2\times l_c^m$ ($\rho=60\%$) up to $4\times l_c^m$($\rho=30\%$) at $l_c=1.5$ mm. If $l_c^m=5$ mm, the width of a calculated localized zone above the notch changes from $2.8\times l_c^m$ ($\rho=60\%$) up to $3.5\times l_c^m$ ($\rho=30\%$),
- concrete softening is strongly influenced by the statistical distribution of aggregate, volume fraction of aggregate and aggregate shape.
- the calculated increment rate of the width of a localized zone is similar as in experiments.

ACKNOWLEDGMENTS

Research work has been carried out within the project: “Innovative ways and effective methods of safety improvement and durability of buildings and transport infrastructure in the sustainable development” financed by the European Union (POIG.01.01.02-10-106/09-01).

REFERENCES

[1] *Z.P. Bažant Z.P., Planas J.*; Fracture and size effect in concrete and other quasi-brittle materials, 1998, CRC Press LLC, Boca Raton

[2] *Lillu G., van Mier J.G.M*; 3D lattice type fracture model for concrete, Engineering Fracture Mechanics, Vol.70, 2003; p.927-941

[3] *Nielsen A.U., Montiero P.J.M., Gjorv O.E.*; Estimation of the elastic moduli of lightweight aggregate, Cement and Concrete Research, Vol.25, 1995; p.276-280

[4] *Sengul O., Tasdemir C., Tasdemir M. A.*; Influence of aggregate type on mechanical behaviour of normal- and high-strength concretes, ACI Master Journal, Vol.99, 2002; p.528-533

[5] *Kozicki J., Tejchman J.*; Modelling of fracture processes in concrete using a novel latice model, Granular Matter, Vol.10, 2008; p.377-388

[6] *He H.*; Computational modeling of particle packing in concrete, PhD Thesis, Delft University of Technology, 2010

[7] *Kim S.M., Abu Al-Rub R.K.*; Meso-scale computational modelling of the plastic-damage response of cementitious composites, Cement and Concrete Research, Vol.41, 2011; p.339-358

[8] *Shahbeyk S., Hosseini M., Yaghoobi M.*; Mesoscale finite element prediction of concrete failure, Computational Materials Science, Vol.50, 2011; p.1973-1990

[9] *Marzec I., Bobiński J., Tejchman J.*; Simulations of crack spacing in reinforced concrete beams using elastic-plastic and damage with non-local softening, Computers and Concrete, Vol.4, 2007; p.377-403

[10] *Skarżyński Ł, Tejchman J.*; Calculations of fracture process zones on meso-scale in notched concrete beams subjected to three-point bending, European Journal of Mechanics A/Solids, Vol.29, No.4, 2010; p.746-760

[11] *G. Pijauder-Cabot, Z.P. Bažant*; Non-local damage theory, ASCE Journal of Engineering Mechanics, Vol.113, 1987; p.1512-1533

[12] *Bažant Z.P., Jirasek M.*; Non-local integral formulations of plasticity and damage: survey of progress, Journal of Engineering Mechanics, Vol.128, 2002; p.1119-1149

[13] *Bobiński J., Tejchman J., Górski J.*; Notched concrete beams under bending – calculations of size effects within stochastic elaso-plasticity with non-local softening, Archives of Mechanics, Vol.61, 2009; p.1-25

[14] *Skarżyński Ł., Syroka E., Tejchman, J.*; Measurements and calculations of the width of the fracture process zones on the surface of notched concrete beams, Strain, Vol.47, 2011; e319-e322, doi: 10.1111/j.1475-1305.2008.00605.x.

[15] *Gitman I.M., Askes H., Sluys L.J.*; Representative volume: Existence and size determination, Engineering Fracture Mechanics, Vol.74, 2007; p.2518-2534

[16] *Du C.B., Sun L.G.*; Numerical simulation of aggregate shapes of two dimensional concrete and its application, Journal of Aerospace Engineering, Vol.20, 2007; p.172-178

[17] *He H., Guo Z., Stroeven P., Stroeven M., Sluys L.J.*; Influence of Particle Packing on Elastic Properties of Conference, The First International Conference on Computational Technologies in Concrete Structures (CTCS'09), Jeju, Korea, May 24-27, 2009

[18] *Katchanov L.M.*; Introduction to continuum damage mechanics, Dordrecht: Martimus Nijhoff, 1986

[19] *Simo J.C., Ju J.W.*; Strain- and stress-based continuum damage models – I. Formulation. International Journal of Solids and Structures, Vol.23, 1987; p.821-840

[20] *Jirasek M., Marfia S.*; Non-local damage model based on displacement averaging, International Journal for Numerical Methods in Engineering, Vol.63, 2005; p.77-102

[21] *Peerlings R.H.J., de Borst R., Brekelmans W.A.M., Geers M.G.D.*; Gradient enhanced damage modelling of concrete fracture, Mechanics of Cohesion – Frictional Materials, Vol.3, 1998; p.323-342

[22] *Bobiński J., Tejchman J.*; Continuous and discontinuous modeling of cracks in concrete elements, Modelling of Concrete Structures (eds. N. Bicanic, R. de Borst, H. Mang, G. Meschke), Taylor and Francis Group, London, 2010; p.263-270

[23] *Syroka E., Bobiński J., Tejchman J.*; FE analysis of reinforced concrete corbels with enhanced continuum models, Finite Element Methods in Analysis and Design, Vol.47, No.9, 2011; p.1066-1078

[24] *Simone A., Sluys L.J.*; The use of displacement discontinuities in a rate – dependent medium, Computational Methods in Applied Mechanics Engineering, Vol.193, 2004; p.3015-3033

[25] *Bobiński J., Tejchman J.*; Numerical simulations of localization of deformation in quasi-brittle materials with non-local softening plasticity, Computers and Concrete, Vol.4, 2004; p.433-455

[26] *Le Bellĕgo C., Dube J.F., Pijaudier-Cabot G., Gerard B.*; Calibration of nonlocal damage model from size effect tests, European Journal of Mechanics A/Solids, Vol.22, 2003; p.33-46

[27] *Eckardt S., Könke C.*; Simulation of damage in concrete structures using multi-scale models, Computational Modelling of Concrete Structures, EURO-C (G. Meschke, R. de Borst, H. Mang and N. Bicanic, editors), Taylor and Francis, 2006; p.77-89

[28] *van Mier J.G.M., Schlangen E., Vervuurt A.*; Lattice type fracture models for concrete, Continuum models for material microstructure (editor H.B. Mühlhaus), John Wiley & Sons, 1995; p.341-377

[29] *Gitman I.M., Askes H., Sluys L.J.*; Coupled-volume multi-scale modelling of quasi-brittle material, European Journal of Mechanics A/Solids, Vol.27, 2008; p.302-327

[30] *Bažant Z.P., Oh B.H.*; Crack band theory for fracture of concrete. Material Structures, RILEM 16, 1983; p.155-177

[31] *Mihashi H., Nomura N.*; Correlation between characteristics of fracture process zone and tension softening properties of concrete, Nuclear Engineering and Desing, Vol.165, 1996; p.359-376

[32] *Syroka E., Tejchman J.*; Experimental investigations of size effect in reinforced concrete beams without shear reinforcement, Internal Report, Gdańsk University of Technology, 2011

[33] *Scrivener K.L., Crumbie A.K., Laugesen P.*; The interfacial transition zone (ITZ) between cement paste and aggregate in concrete, Interface Science, 411-421, Springer Netherlands, http://dx.doi.org/10.1023/B:INTS.0000042339.92990.4c, 2004

[34] *Mondal P., Shah S.P., Marks L.D.*; Nanomechanical properties of interfacial transition zone in concrete, Nanotechnology in Construction 3, Springer, 2009; p.315-320

[35] *Ortiz M., Pandolfi A.*; Finite-deformation irreversible cohesive elements for three-dimensional crack-propagation analysis, International Journal for Numerical Methods in Engineering 44, 1999; p.1267-1282

[36] *Belytschko T., Moes N., Usui S., Parimi C.*; Arbitrary discontinuities in finite elements, International Journal for Numerical Methods in Engineering 50, Vol.4, 2001; p.993-1013

[37] *Simone A., Sluys L.J.*; The use of displacement discontinuities in a rate-dependent medium, Computer Methods in Applied Mechanics and Engineering 193, 2004; p.3015-3033

[38] *Moonen P., Carmeliet J., Sluys L.J.*; A continuous-discontinuous approach to simulate fracture processes, Philosophical Magazine 88, 2008; p.3281-3298